A PZT Array Actuator Using Buckling Strain Amplification and Preload Mechanisms

Citation: Torres, James, et al. "A PZT Array Actuator Using Buckling Strain Amplification and Preload Mechanisms." ASME 2011 Dynamic Systems and Control Conference and Bath/ASME Symposium on Fluid Power and Motion Control, Volume 2, 31 October - 2 November, 2011, Arlington, Virginia, ASME, 2011, pp. 25–32. © 2011 ASME

As Published: http://dx.doi.org/10.1115/DSCC2011-6070

Publisher: ASME International

Persistent URL: http://hdl.handle.net/1721.1/118799

Version: Final published version: final published article, as it appeared in a journal, conference proceedings, or other formally published context

Proceedings of the ASME 2011 Dynamic Systems and Control Conference
DSCC2011
October 31 - November 2, 2011, Arlington, VA, USA

DSCC2011-6070

A PZT ARRAY ACTUATOR USING BUCKLING STRAIN AMPLIFICATION AND PRELOAD MECHANISMS

James Torres
Devin Neal, H. Harry Asada
Mechanical Engineering
Massachusetts Institute of Technology
Cambridge, MA 02139
jtorres9@mit.edu

ABSTRACT

Displacement amplification mechanisms have been a topic of research for piezoelectric actuators for decades to overcome their significantly small strain, but still utilize their high power density, force, and efficiency. This paper further analyzes a nonlinear buckling mechanism to improve its efficiency, defined as the ratio of mechanical work output of the buckling actuator to the mechanical work output of the PZT actuator , as well as, employing two methods, preload and loading conditions, that improve its work output per cycle. This is accomplished by running a numerical analysis of the geometry of the flexure joints in the buckling mechanism which found a maximum mechanical efficiency of 48%. The preload is applied using shape memory alloy wire to exploit the low stiffness of the super elastic regime; which in turn allows a larger work output due to a loading condition supplied by a novel gear design. Finally, a prototype was fabricated to provide a baseline of comparison against these concepts.

INTRODUCTION

Piezoelectric actuators, such as lead zirconate titanate, PZT, stacks, have several desirable properties, including high bandwidth and large power density. The limited strain, which is on the order of 0.1%, however, has limited their widespread use. Several techniques have been developed to overcome this limitation and utilize piezoelectric materials attractive aspects; such as, the use of displacement amplification methods or friction drives excited at ultrasonic frequencies. Ultrasonic motors, due to their exploitation of piezoelectric actuators' high bandwidth, allow for fast response time and easy control, but they are limited to small loads, high frequency power supplies, and short lives [1]. Displacement amplification methods, usually through the use of cantilevers, have been explored extensively. They have been used in everything from cycloid motors [2] to clutching devices [3] to helicopter rotor controls [4]. Compliant flexure mechanisms are popular because of their high precision, repeatability, ease of fabrication, and feasibility. Significant analysis has gone into optimizing these flexures to maximize the output efficiencies relative to work input, overall mass, and overall cost. [5]

While most of the displacement amplification methods are cantilevered and require at least two layers of amplification to provide useful displacement; this paper focuses on the further analysis and a possible application of the non-linear flextensional "buckling" mechanism described here [6, 7]. This paper shows the benefit that the buckling mechanism provides, while under properly preloaded conditions, is a more efficient loading of the PZT stack such that there is an increase in the work output per cycle. Using an array of these buckling mechanisms in a motor, fundamentally similar to a harmonic drive, utilizes a PZT actuator better than the ultrasonic friction drives. This is largely due to the array of PZT actuators supplying the load directly to a gear relying on the normal force to transmit the work, as opposed to friction.

The principle of the loading conditions is discussed first. This is followed by the details of the gear design. Next, an analysis of the buckling actuator explains how it would capitalize on the optimal loading conditions. Then, an in depth model of the stiffness characteristics of the actuator is described. Finally, a prototype of a motor and future work is discussed.

PRINCIPLE AND METHODS OF EFFICIENT LOADING

Two boundary conditions that constrain the stack actuator limit the loading conditions and subsequently affect the work output per cycle. First, the stack has an acceptable voltage band; and second, it cannot be placed in tension. Both of these

constraints are to prevent permanent damage to the stack actuators. Furthermore, the loading conditions of the PZT actuator can greatly affect the work output per cycle. Allowing a change in motion, force, and voltage simultaneously reduces the work output of a single stroke of the stack actuator. When the actuator is activated, the trajectory it follows is dependent on the load. As shown in Fig. 1, this trajectory can be complex based on the dynamics, (1'), or, in the ideal case, simple, (1). Note that trajectory (1'), is merely an example, and could be significantly different dependant on the impedance of the load itself. In the ideal case, trajectory (1), the load is considered to be an infinite stiffness, which allows no displacement for any load. Consequently, it becomes imperative for the loading cycle efficiency that the output load during the activation be as stiff as possible. The following equation defines the work output, W_o, as the line integral of the trajectory: (1), (2), (3), and where δ_{max} and F_b are the maximum free displacement and the blocking force of the PZT actuator, respectively.

$$W_o = \oint F_{PZT} \cdot dx = \frac{F_b \delta_{\max}}{2} \quad (1)$$

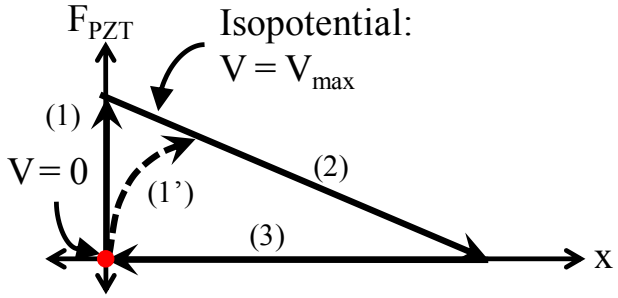

FIGURE 1. LOADING TRAJECTORY THAT MAXIMIZES THE WORK OUTPUT PER CYCLE OF PZT STACK WITHIN THE BOUNDARY CONDITIONS

Zero Stiffness Preload – Shape Memory Alloy As A Preloading Device

There are several benefits to preloading the stack actuator, particularly an approximately zero stiffness preload. Preloading is most commonly used to reduce or remove the internal clearance of surface contact, which in turn increases the cyclic life of that mechanism. Furthermore, the Hertzian contact compliance is a non-linear function with the force applied that is roughly inversely proportional to the cube root of the force. An increase in preload force will, therefore, decrease the parasitic contact compliance, which is in series with the actuator. This effective stiffness of both the PZT stack and the surface contact then approaches the stiffness of the just the PZT actuator itself, and allows the actuator to provide its maximum displacement. Furthermore, beyond these typical benefits of preloading some PZT actuators have been shown to perform more efficiently under pre-stressed conditions [8].

Most significantly, however, a constant preload allows for a PZT stack to effectively handle a tensile load. This is achieved by taking advantage of two properties. The first property is the ability of PZT stacks to extend their full stroke while under constant load. This is most easily demonstrated by applying a constant load, such as a weight, and then inputting a sine wave signal at a quasi-static frequency to the stack actuator while measuring the peak-to-peak displacement. As the weight is increased, the overall position moves, but the peak-to-peak displacement remains approximately constant. The second property is the super elastic regime of shape memory alloy, SMA. Between approximately 1% and 11% strain the stress of SMA increases from 520 MPA to 600 MPa. A shape memory alloy wire loaded until the stress is within the super-elastic regime, typically around 560 MPa, and wrapped around the PZT actuator provides force proportional to the total cross sectional area of the wire and a stiffness of approximately 0.1% of the stack.

Preloaded Loading Cycle

A preload, with zero stiffness, equal to the blocking force shifts the force displacement origin along the zero isopotential, as shown in Fig. 2. The stack-preload assembly can be placed in tension, unlike the lone stack actuator, which doubles the total possible work output per cycle. The tensile output force is possible because as a tensile load is applied to the assembly, the piezoelectric actuator is able to relax as the preload is lessened because the preload is shifted from being applied to the PZT stack to the output. The desired cycle is similar to the non-preloaded case with the exception of the addition of the tensile load. The enumerated preloaded loading trajectories in Fig. 2 go as follows, (1) constrain position and charge, (2) constrain voltage and displace, (3) constrain position and discharge, and (4) constrain voltage and displace. Note this reduces the types of constraints from three (voltage, position and force) to just two (voltage and position). This simplifies design as it allows force to be inherently causal in the system and requires a very simple controller for the voltage signal.

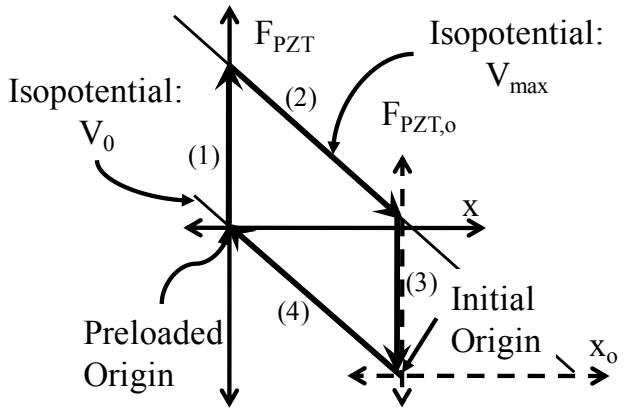

FIGURE 2. PRELOADED PZT ACTUATOR LOADING TRAJECTORY THAT INCREASES THE WORK OUTPUT PER CYCLE.

Gear Tooth Design

The loading trajectory can increase the work output, but it must do so in a useful way. Figure 3 shows several preloaded PZT stacks with their output nodes in the track of a slotted gear. This gear has geometry specifically intended to load the PZT actuator along the preloaded loading trajectory. The gear is portrayed as a rack and pinion but could easily be applied to a rotational gear. The flat plateaus and valleys per cycle correspond to the charging and discharging portions of the trajectory and are ideally considered to be infinitely stiff so that trajectories (1) and (3) are vertical. The enumerated points in Fig. 2 correspond to the four PZT actuators in Fig. 3. Stacks (1) and (3) are constrained so as they charge and discharge, respectively, their displacement is held constant. Note it is assumed but not shown, that all of the stacks have been preloaded by SMA to ensure the trajectory in Fig. 2 can be followed. Due to the PZT stack's high bandwidth, on the order of 10s of kHz, and the loading frequencies of less than 100 Hz, it can be assumed that they are quasi-statically loaded, and therefore, reliably adhere to the desired trajectory. Furthermore, the precise geometry of the slot gear, the slope of the incline in particular, can greatly affect the linear speed and force, or angular speed and torque in the rotational gear. The lengths of the plateaus are based on the peak current and speed of the gear, such that the power source is able to charge the stack actuators completely within the time span. As the current increases, the time to charge decreases and thus the plateaus can be shorter.

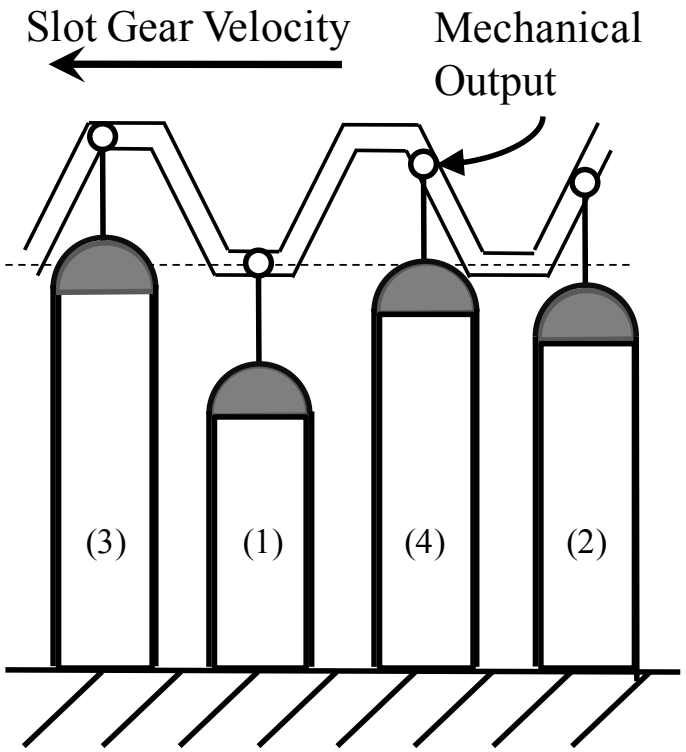

FIGURE 3. SLOT GEAR DESIGN ALONG WITH FOUR PZT ACTUATORS IN VARIOUS LOADED POSITIONS

BUCKLING ACTUATOR STIFFNESS ANALYSIS

At first glance this design seems very similar to the ultrasonic motors already on the market. Likewise, it seems limited in the same way. The tolerance and machinability of the gear is not practical, as the manufacturing process would require sub-micron level accuracy to achieve a viable gear. The gear tooth height would be on the order of tens of microns. Furthermore, any typical loads would cause significant deflection in the system and greatly degrade performance.

This is precisely the intended application of the previously mentioned displacement amplification mechanisms. A larger stroke actuator with displacements on the order of millimeters can withstand losses due to machine tolerances, deflections, and alignment slop. Minimizing these losses is important to maintain a high efficiency. As stated before, this paper focuses on a specific amplification method described here [6, 7]. Figure 4 shows a modified version of the actuator in both the a) resting position, and b) a displaced configuration. Semi-circular caps on each end of the stacks would be the terminals for the preload. Not explicitly shown is the SMA wire which would be wrapped around the caps of each individual PZT actuator.

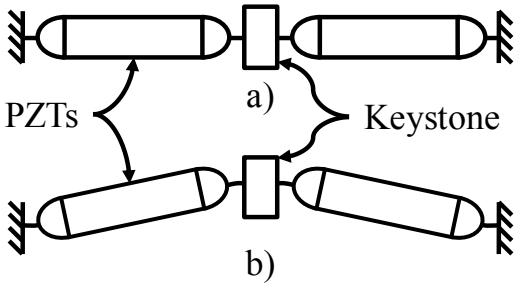

FIGURE 4. BUCKLING MECHANISM CONTAINING A PAIR OF PRELOADED PZT STACKS IN BOTH THE NEUTRAL AND DISPLACED CONFIGURATION

Simple Spring Model

A simple spring model for the stack actuator is first used as a matter of comparison and to gain insight for the mechanical design, particularly how the parallel and series stiffnesses affect the output force and displacement. Figure 5 shows a model of a force source, with input force f, and spring, with stiffness k_p, in parallel followed by a spring in series, with stiffness k_s. The output node, shown in red, has a displacement, z, and force, F_o. The output force as a function of the input force and displacement is:

$$F_o = \frac{k_{eff}}{k_p} f - k_{eff} z \tag{3}$$

Where the effective stiffness, k_{eff}, is defined as the series sum of the two springs:

$$k_{eff} \equiv \left(\frac{1}{k_s} + \frac{1}{k_p} \right)^{-1} = \frac{k_s k_p}{k_s + k_p} \tag{4}$$

Equation (3) shows that as the parallel spring stiffness approaches zero, the output force follows the input exactly, note the k_p term cancels within the k_{eff}. Physically this doesn't help, however, because in the actual system the parallel stiffness is related to the stack actuator properties and is not within the design space. Therefore, to improve the work output, the serial stiffness should be much larger than the parallel stiffness so the effective stiffness is approximately equal to the parallel stiffness alone.

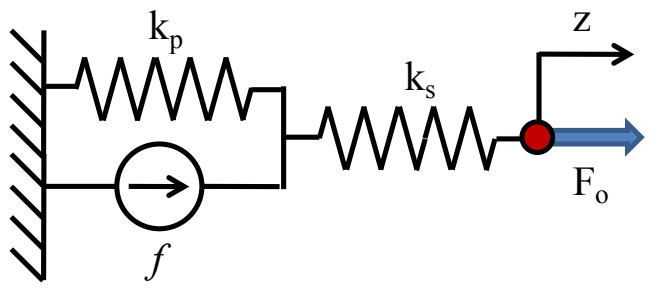

FIGURE 5. SIMPLE LINEAR SPRING MODEL FOR COMPARISON

Non-Linear Spring Model

To obtain an understanding of the expected forces and displacements, a lumped parameter model is used, modeling both the compressive and bending stiffnesses of the joints and representing the PZT stacks as a spring and force source in parallel. It is convenient to take advantage of the symmetry of the mechanism about the y-axis and analyze only one-half. The joints are assumed to be identical and the bending stiffness is based on lumped model, see Annex A for the derivation of the bending stiffness, k_b.

Figure 6 contains a schematic of buckling actuator, where k_j is the compressive joint stiffness, k_{PZT} is the stiffness of the PZT stack, defined as the blocking force divided by the free displacement, and k_b is the bending stiffness. Furthermore, F_{PZT} is the force applied by charging the PZT actuator. Due to symmetry the output node, shown in red, is constrained to the y-axis. Thus, when the stack actuator is charged and subsequently extended the buckling actuator is forced to "buckle" and push upwards (or downwards). The overall extension, x, can be related to the original length, L, and the output displacement, y, using simple geometry.

$$x \approx \frac{y^2}{2L} \tag{5}$$

Equation 5 is valid under the small angle approximation. As the output node moves upward, the force along the axial direction of the PZT stack is rotated upward as well. This angle, θ, is defined by:

$$\sin\theta = \frac{2Ly}{2L^2 + y^2} \tag{6}$$

and,

$$(1 - \cos\theta) = \frac{y^2}{2L^2 + y^2} \tag{7}$$

The output force, F_y, is therefore, the y-component of the force along the axis of the PZT stack subtracted by the force to bend and compress the joint. More explicitly:

$$F_y = \frac{k_l}{k_{PZT}} F_{PZT} \sin\theta - \left((1 - \cos\theta) k_l + k_b \right) y \tag{8}$$

Where k_l is defined as the series sum of the three axial springs:

$$k_l \equiv \left(\frac{1}{k_{PZT}} + \frac{2}{k_j} \right)^{-1} = \frac{k_{PZT} k_j}{2k_{PZT} + k_j} \tag{9}$$

Note that the output force, F_y, is half of the total output force as the two halves are connected in parallel. For simplicity, this paper looks at the contribution due to just one PZT actuator, recognizing that the force and the work output scales linearly with the number of stacks. From the previous model, it is expected that the serial stiffnesses, k_j, should be large compared and the bending stiffness, k_b, should be small when compared to the stack stiffness, k_p. Equation (8) supports these expectations. The first part of the equation is identical to Eq. (3) save for the trigonometric term caused by the rotation of the PZT stack. The second half contains a similar trigonometric term, as well as, an extra term from the bending stiffness. While the shape of the force-displacement curve is highly dependent on the relative magnitudes of the three stiffnesses, k_j, k_{PZT}, and k_b, Figure 7 shows two typical curves for the "on" and "off" conditions, where the force input is F_b and 0, respectively.

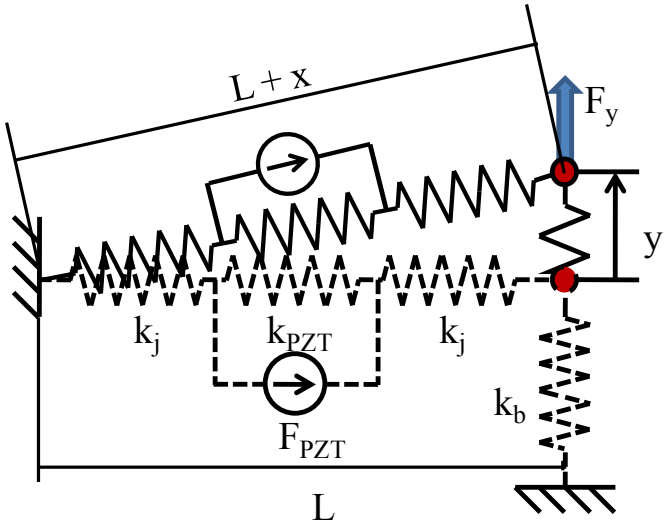

FIGURE 6. SPRING MODEL OF BUCKLING MECHANISM

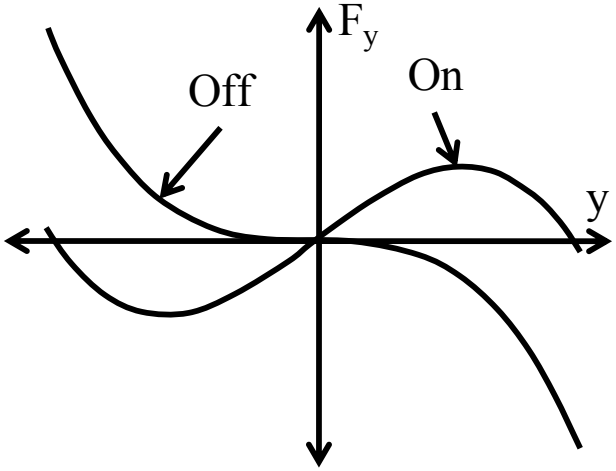

FIGURE 7. FORCE-DISPLACEMENT CURVE OF THE BUCKLING MECHANISM

Numerical Analysis of Joint Dimension Optimization

Looking at Eq. (8), Fig. 6, and the conclusions from the simple spring system, it is clear that in the ideal situation, the compressive joint stiffness, k_j, would be infinite and the bending stiffness, k_b, would be zero. Unfortunately, these two stiffnesses are coupled due to their dependence on the joint geometry. At one extreme, if the length of the joint is long, such that both the bending and compressive stiffnesses are small; the joint would offer little resistance in the output direction, but would absorb most, if not all, of the PZT actuators' displacement in compression. The other extreme, if the length is small, such that both the bending and compressive stiffness are large; the joint would compress very little, but would have a tremendous resistive force due to the bending stiffness in the output direction. Therefore, there is a middle ground that can be considered optimal. The ultimate goal of the displacement mechanism is to transmit mechanical energy from the PZT actuator to the output. Therefore, the optimal joint dimension will maximize the work output efficiency, η, defined as the work output, W_o, divided by the work input, W_i.

$$W_i \equiv \oint F_{PZT} \cdot dx \tag{10}$$

$$W_o \equiv \oint F_y \cdot dy \tag{11}$$

$$\eta \equiv \frac{W_o}{2W_i} \tag{12}$$

The factor of two in Eq. (12) is a result of the two input cycles per output cycle. Note that the bounds of both integrals are dependent on the joint stiffness, as well, because only the longest cycle that is always producing positive work is considered. Consequently, the bounds on the work output, $\pm y_c$, satisfy the equation:

$$\frac{k_l}{k_{PZT}} F_b \sin\theta_c = \left(\left(1-\cos\theta_c\right)k_l + k_b\right)y_c, y_c > 0 \tag{13}$$

Where θ_c is:

$$\theta_c \equiv \theta\left(y_c\right) \tag{14}$$

Likewise the bound for the work input, x_c, is:

$$x_c \equiv x\left(y_c\right) \approx \frac{y_c^2}{2L} \tag{15}$$

An NEC-Tokin PZT stack, AE1010D44H40F, which has the following specifications: length of 40 mm, a cross-sectional area of 10 mm by 10 mm, 100 mm^2, a blocking force of 3500 Newtons, and a free displacement of 42.0 μm [9] was used for the purpose of the numerical analysis. The joint is assumed to be made of steel with a thickness of 12.5 mm and a minimum possible width of 0.2 mm. This resultant optimal joint length is 2.2 mm which has a mechanical efficiency of 48%. Figure 8 shows the force-displacement trajectory of one complete cycle.

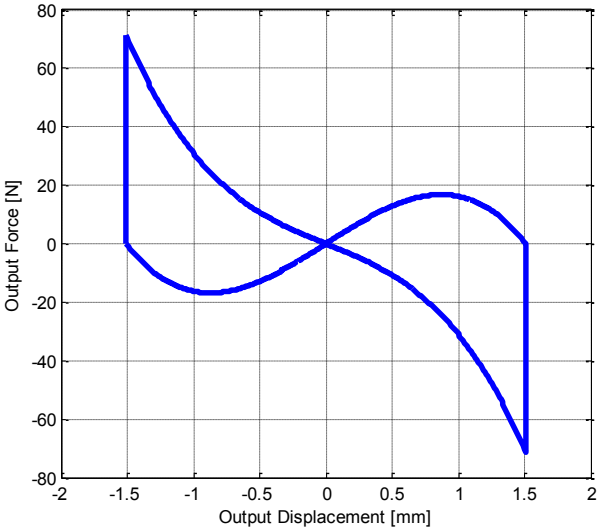

FIGURE 8. FORCE-DISPLACEMENT CURVE FOR THE OPTIMAL BUCKLING MECHANISM, OPTIMIZING MECHANICAL EFFICIENCY FOR THE AE1010D44H40F NEC-TOKIN PZT STACK

Loading Cycle of the Integrated Buckling Mechanism

The increased stroke and ability to displace bi-directionally of the buckling mechanism allows the gear's size to increase within practical machining limits. Furthermore, as Fig. 9a shows, the tooth geometry is modified so there are now four constant regions where the PZT actuator can charge or discharge at constant displacement. Figures 9b and 9c show the points on the gear tooth that correspond to points on the PZT actuator and buckling mechanism force-displacement curves. The points are labeled for one full cycle of the PZT actuator, which relates to one half-cycle of the buckling mechanism and gear. The gear is symmetric about the dotted line, the neutral point of the buckling mechanism, and the buckling mechanism force-displacement curve is symmetric about the origin.

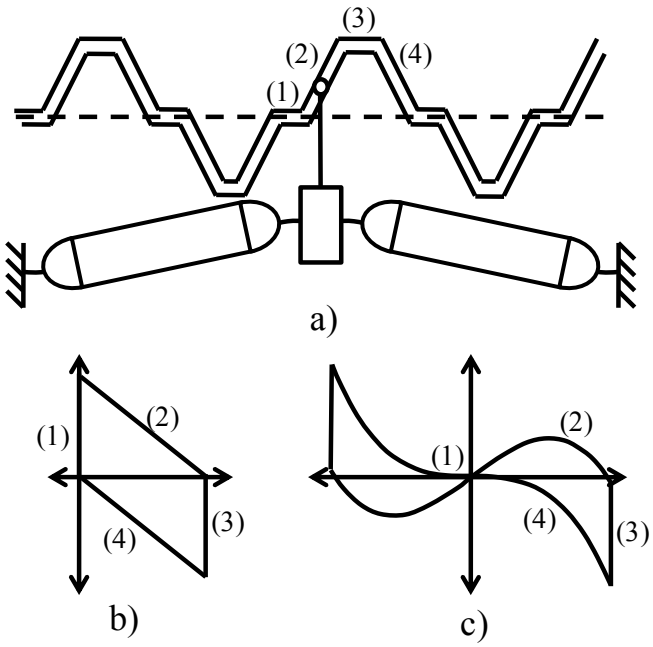

FIGURE 9. A SCHEMATIC OF THE SLOT GEAR INTERFACING WITH A BUCKLING MECHANISM ALONG WITH THE CORRESPONDING FORCE-DISPLACEMENT CURVES FOR THE PZT ACTUATOR AND THE BUCKLING MECHANISM

PROTOTYPE AND FUTURE WORK

As an application of this work, a prototype motor was built to confirm the feasibility and capabilities of the buckling mechanism; particularly how the buckling mechanism performs dynamically. This initial prototype does not contain the SMA preload, and uses the previous method explained here [6]. The motor, a schematic shown in Fig. 10 and the actual prototype shown in Fig. 11, consists of three buckling mechanisms forming and equilateral triangle concentric with a slot gear, note the gear is not shown in Fig. 11.

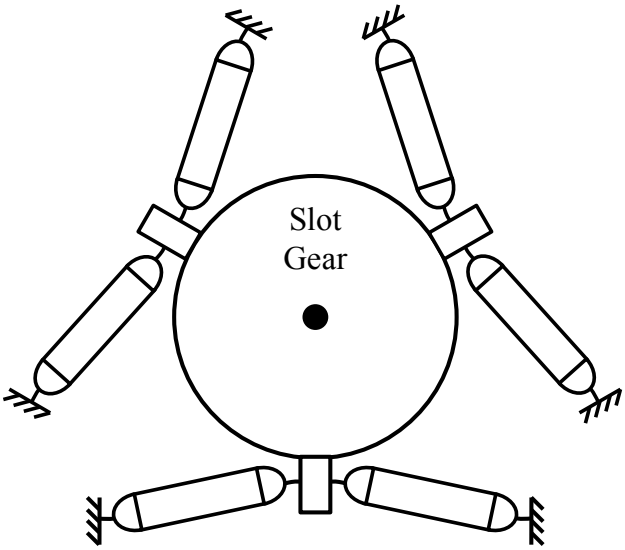

FIGURE 10. SCHEMATIC OF THE MOTOR WITH THREE BUCKLING MECHANISMS SURROUNDING THE OUTPUT GEAR

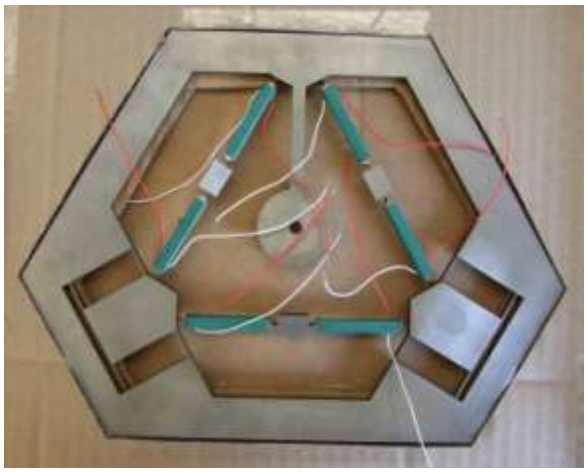

FIGURE 11. MOTOR PROTOTYPE WITH THREE PAIRS OF BUCKLING MECHANISMS

CONCLUDING REMARKS

This paper focused on the benefits of two methods to improve the work output of a PZT buckling mechanism, a preload to allow and a gear tooth design that would exploit a more efficient loading trajectory. Furthermore, the buckling mechanism was analyzed to maximize the mechanical efficiency of the flexure based design. Finally, a prototype was fabricated that will allow deeper comparison of these methods.

REFERENCES

[1] Uchino, K. 1989. "Ultrasonic Motors". *Japan Society for Precision Engineering*, 55, pp. 485.

[2] Hayashi, I., Iwatsuki, N., Kawai, M., Shibata, J., and Kitagawa, T. 1991. "Development of a Piezoelectric Cycloid Motor". *Mechatronics*, 2(5), pp. 433-444.

[3] Thornley, J. K., Preston, M. E., and King, T. G. 1993. "A very High-Speed Piezoelectrically Actuated Clutching Device". *Mechatronics*, 3(3), pp. 295-304.

[4] Prechtl, E., and Hall, S. 1999. "Design of a high efficiency, large stroke, electromechanical actuator". *Smart Materials and Structures*, 8, pp. 13-30.

[5] Lobontiu, N., and Garcia, E. 2003. "Analytical Model of Displacement Amplification and Stiffness Optimization for a Class of Flexure-Based Compliant Mechanisms". *Computers and Structures*, 81, pp. 2797-2810.

[6] Neal, D., and Asada, H. 2010. "Phased-Array Piezoelectric Actuators Using a Buckling Mechanism Having Large Displacement Amplification and Nonlinear Stiffness". *International Conference on Robotics and Automation*, May, pp. 1661-1667.

[7] Neal, D., and Asada, H. 2010. "Dynamic Performance of Nonlinear 100X Displacement Amplification Piezoelectric Actuator". *Dynamic Systems and Controls Conference*.

[8] Zhou, D., Kamlah, M., and Munz, D. 2004. "Effects of Uniaxial Prestress on the Ferroelectric Hysteretic Response of Soft PZT". *Journal of the European Ceramic Society*, 25, pp. 425-432.

[9] www.nec-tokin.com, "Multilayer Piezoelectric Actuators," March 2011.

ANNEX A

DERIVATION OF THE BENDING STIFFNESS

The bending stiffness of the buckling mechanism is a beam bending problem with constraints shown in Fig. 12. The two identical joints are assumed to have a Young's modulus, E, inertia, I, length, L_j, and thickness, t. The rigid bar in the center has length L. A load, P, is applied and causes a displacement, Δy. The stiffness, k_b, is defined as:

$$k_b \equiv \frac{P}{\Delta y} \tag{16}$$

For small displacements, such that a first order approximate of trigonometric functions is accurate, the stiffness becomes:

$$k_b = \frac{6EI}{\left(3L + 4L_j\right)L_j^{\,2}} \tag{17}$$

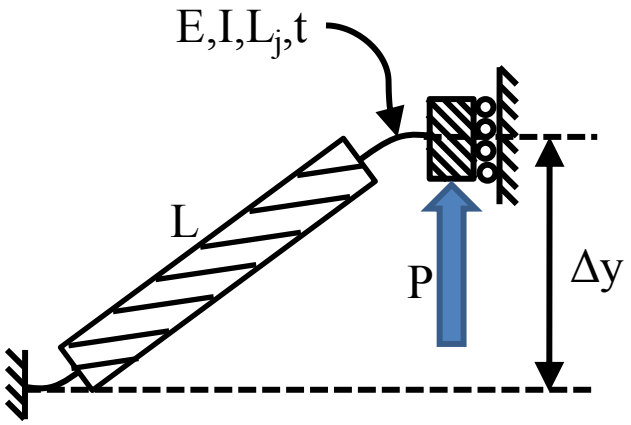

FIGURE 12. BENDING STIFFNESS BOUNDARY CONDITIONS